NANO LETTERS

LETTER

pubs.acs.org/NanoLett

Ultrasmall Silver Nanopores Fabricated by Femtosecond Laser Pulses

F. Bian,[†,§] Y. C. Tian,[†,§] R. Wang,[†] H. X. Yang,[†] Hongxing Xu,[†,‡] Sheng Meng,[*,†] and Jimin Zhao[*,†]

[†]Beijing National Laboratory for Condensed Matter Physics and Institute of Physics, Chinese Academy of Sciences, Beijing 100190, China

[‡]Division of Solid State Physics, Lund University, Lund 22100, Sweden

Supporting Information

ABSTRACT: Ultrasmall nanopores in silver thin films with a diameter of about 2 nm have been fabricated using femtosecond laser ablation in liquid. Ultrafast laser pulse ablation generates highly nonequilibrium excited states, from which silver thin films emerge and progressively grow with the assistance of capping agent molecules. During this growth process, capping agent molecules are enclaved within the film, leaving individual ultrasmall pores in the thin film. Our first-principles calculations show that the pore size is critically determined by the dimension of the confined molecules. Our approach advances the capability of optical methods in making nanoscale structures with potential applications in areas such as near-field aperture probes, imaging masks, magnetic plasmonic resonances, and biosensing with individual nanopores.

KEYWORDS: Nanopore, laser ablation in liquid, femtosecond, capping agent molecule, first principles, molecular interaction

Separable individual nanopores are of interest in many areas such as plasmon-related nanophotonics,[1−3] local probe imaging masks,[4] and single-molecule biosensing.[5] For instance, it has been shown that individual ultrasmall nanopores are needed for rapid sensing of single DNA molecules.[5,6] Individual nanopores have been fabricated on insulating Si_3N_4 using ion beam lithography,[7] on SiO_2 using electron beam lithography,[8] and most recently on graphene using electron beam drilling.[9,10] Similar technologies applied to metallic materials have been used to make nanopores with the smallest pore diameter of slightly less than 10 nm.[11] Optical methods have also been attempted, and the smallest hole was achieved with femtosecond near-field laser ablation with a diameter of 6 nm on gold.[12] Herein we report nanopores on a metallic material down to a size of about 2 nm in diameter fabricated by a novel optical method based on femtosecond laser ablation in liquid (LAL).

Despite the fact that propagation of light always introduces diffraction, which imposes stringent constraints on the spatial resolution that light effectively reaches, sustained efforts have been devoted to novel methods of using photons to produce solid state structures down to subwavelength and nanometer scales. Successful methods associated with these efforts can be classified into three categories: (1) methods through nonlinear optical effects (i.e., with assistance of multiple photons),[13] (2) methods with assistance of nanoscale metallic tips or other structures,[14] and (3) methods with assistance of atoms/molecules in gaseous[15] or liquid phases.[16,17] However, so far all these approaches are facing great challenges in making ultrasmall structures at the few nanometer scale, especially in practice with metals, due to the presence of aforementioned spatial limits of light diffraction and ultrasensitive plasmonic response of metals.

Laser ablation in liquid, which belongs to the third category mentioned above, is a recently developed and rapidly evolving method[18] to produce metal nanoparticles. In this approach, an ultrafast laser beam is focused onto a metal plate, which is immersed in deionized water or aqueous chemical solutions for minutes or hours, to produce metal nanoparticle suspensions. In this method, the problems of agglomeration in gas-phase processes and the use of toxic precursors in chemical reduction methods are avoided,[18] making it appropriate for biosensing and for making advanced functional materials.[19] The effects of laser pulse fluence,[20] central wavelength,[21] temporal pulse width,[22] and surfactant properties[20,23] on the particle formation have been investigated, all of which mainly concern with the particle size and production rate.[24] However, morphologies other than near-spherical shapes have rarely been reported, and there have been no reports on making metallic nanostructures as small as a few nanometers. Meanwhile light-illuminated chemical reduction[16,17,25,26] and thermal processing[27] have been used to make various nanoscale metal structures, such as nanowires,[26] nanoprisms,[17] nanorings,[28] and nanocages.[29] So far nanostructures smaller than 5 nm, especially metallic nanopores, have *not* been achieved. In this work we report a step toward advancing the capability of optical methods to make the ultrasmall metal structures with femtosecond laser pulses. We combine the advantages of both the highly energetic excitation of ultrafast laser ablation and the confining functions of capping agents from chemical reduction methods. Experimental data together with first-principles calculations clearly reveal the mechanism of ultrasmall nanopore formation via progressive enclavement of capping agent molecules. Our revised laser ablation method can routinely produce ultrasmall nanopores at a density of $\sim 2000/\mu m^2$, which is not possible using either regular LAL or chemical reduction methods alone, nor any other currently available top-down technologies.

Intense amplified femtosecond laser pulses were used to ablate a silver plate ($10 \times 10 \times 0.2$ mm^3) immersed in an aqueous solution of capping agents. The 0.2 mm thick pure silver

Received: May 7, 2011
Revised: June 21, 2011
Published: June 30, 2011

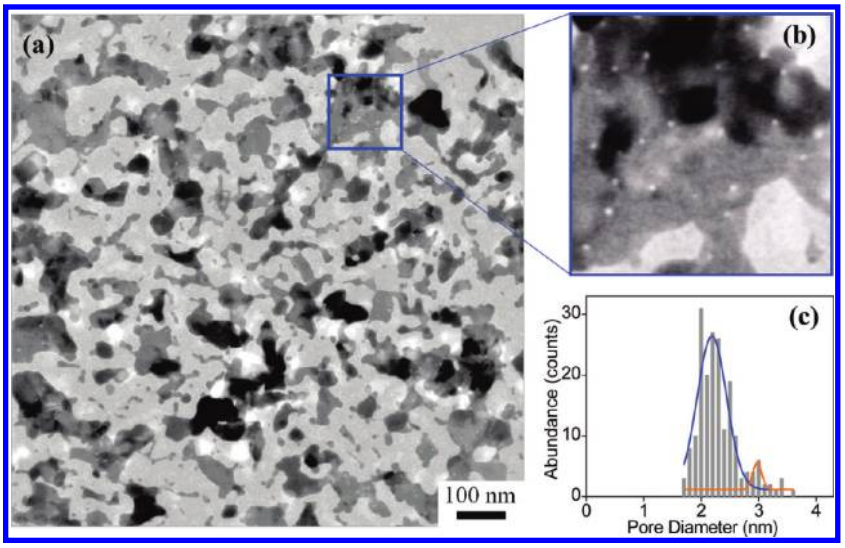

Figure 1. Morphology and size distribution of the ultrasmall silver nanopores produced by femtosecond laser ablation in a capping agent solution. (a) Large area TEM image of the silver thin films. (b) Zoom-in view of the silver film with dense ultrasmall nanopores clearly visible. (c) Histogram of the diameter distribution of the nanopores in (a). The blue and yellow curves are Gaussian fits of the diameter distribution as a guide to the eye.

(99.99%) plates were prepared by mechanical polishing and then cleaned three times with deionized water at room temperature. For each experiment one silver plate was placed on the bottom of a culturing dish, which was filled with aqueous capping agents in deionized water. The solution's depth above the silver plate was 4 mm. Our laser beam had a central wavelength of 800 nm, an average power of 700 mW, a repetition rate of 250 kHz, and a pulse duration of 80 fs (Micra seeded RegA-9050 Ti:sapphire laser amplifier, Coherent Inc.). The linearly polarized laser beam had a $1/e$ amplitude radius of 2.7 mm and was focused using a convex lens with a focal length of 50.8 mm onto the top surface of the silver plate. Throughout our experiment each plate was ablated continuously for 10 min, during which the whole culturing dish was laterally translated underneath the laser spot manually and smoothly so that texturing effects were avoided. We added 0.3 mM sodium citrate ($Na_3C_6H_5O_7$, Alfa Aesar) and 0.1 mM poly(vinylpyrrolidone) (PVP, $[-C_6H_9NO-]_n$, average molecular weight 40000, Aldrich), which have been used in chemical reduction methods to make nanowires and nanoprisms,[26] to 11.03 mL of deionized water (Milli-Q, Millipore Co.) to make a mixed solution before laser ablation. The major effect of PVP, a water-soluble polymer which coats the surfaces of the silver particles, is to prevent the produced silver nanoparticles from aggregation, which is illustrated in Figure S1 of the Supporting Information and discussed in refs 26 and 27. The role of sodium citrate is such that citrate anions selectively attach to the (111) facets of the silver particles only allowing the silver particle to grow within the (111) plane.[16,27]

To observe the morphology and gain insight of the formation mechanism of the nanopores, we took transmission electron microscopy (TEM) images with a transmission electron microscope (JEM-2010, JEOL 200 kV). The samples were routinely prepared by depositing a drop of suspension containing silver nanoparticles onto a copper mesh coated with carbon film and letting them dry completely in an electronic drying cabinet in room temperature. Care was taken such that room light did not reach the samples during their drying process. Atomic force microscopy (AFM) images are also obtained using an atomic force microscope (SPI4000/SPA300HV, Seiko Instruments Inc.).

The calculations reported here were performed with the SIESTA code.[30] The computational settings are briefly introduced as follows. We use pseudopotentials of the Troullier–Martins type[31] to model the atomic cores, the PBE form of the exchange-correlation functional,[32] and a local basis set of double-ζ polarized orbitals (including 15 numerical atomic orbitals for Ag; 13 orbitals for C and O; 5 orbitals for Na and H). An auxiliary real space grid equivalent to a plane-wave cutoff of 120 Ry is used for the calculation of the electrostatic (hartree) term. A (3×3) supercell is used to model citrate molecule adsorption on the Ag(111) surface, with the Monkhorst–Pack k-point sampling of (3×3) in the surface Brillouin zone. Solvent molecules are not currently included in the model structures, since they participate in weaker interactions including hydrogen bonding and van der Waals forces; investigations of their influence are under way. For geometry optimization, a structure is considered fully relaxed when the magnitude of forces on the atoms is smaller than 0.04 eV/Å.

A typical TEM image of such a film is illustrated in Figure 1a. We observe a distribution of dense, similar-sized, and ultrasmall nanopores, with a typical pore density of $\sim 2000/\mu m^2$, more clearly seen in the zoom-in view in Figure 1b. These silver nanopores have extremely small pore sizes and a very narrow diameter distribution, of which the abundance statistics corresponding to the pores in Figure 1a is shown in Figure 1c. Two Gaussian curves have been used to fit the mean pore sizes. A major mean pore size of 2.3 nm and a second one of 3.1 nm are found. Although nanowires and nanoprisms have been routinely made with the same capping agents in chemical reduction methods, nanopores have not been reported to the best of our knowledge. We explore the formation mechanism of these nanopores in detail and discuss the unique aspect of our approach in the following.

Figure 2a shows multiple silver nanopores that coexist on a single thin film. Together with TEM images in Figure 1, we found that these pores are similar to each other, spatially uncorrelated, and stable at room temperature. The nanopores are separated with a typical distance of ~20 nm, much smaller compared with the light wavelength used (800 nm). Figure 2b is the high resolution TEM image of two of the nanopores manifesting

dx.doi.org/10.1021/nl201529d |*Nano Lett.* 2011, 11, 3251–3257

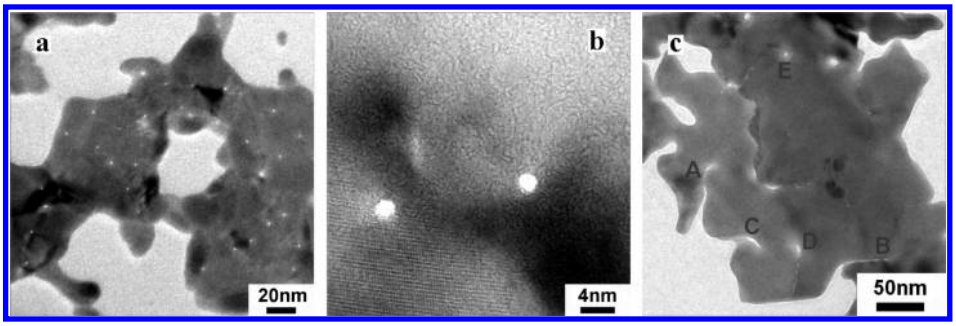

Figure 2. TEM images showing the progressive growth mechanism of nanopore formation. (a) TEM image of Ag thinfilm after LAL shows multiple nanopores coexisting in a single film: they are dense, spatially uncorrelated, and stable at room temperature. (b) High-resolution TEM image of two of the nanopores showing the typical nearly perfect circular pore shapes with smooth pore edges and no aggregation of atoms around the edge. (c) Progressive evolution sequence, marked by A → B → C → D → E, of the enclosing enclaves, toward a stabilized round-shaped nanopore (E).

typical nearly perfect circular pore shapes, with smooth pore edges and no aggregation of atoms at the edge. These are in sharp contrast to the relatively large holes made by other laser ablation methods with[12] or without[33] a metallic tip, where edge-atom aggregation shows up.

Two scenarios might be responsible for the formation of these extremely small nanopores. The first scenario is light-induced atom *disaggregation*, where pores are formed as a result of some atoms leaving the film due to exposure to light through either nonthermal femtosecond ablation (optomechanical effects)[34] or plasma-related heating and breakdown effects (thermal effects).[35] The second scenario is progressive *growing process*, where silver components produced from laser excitation grow and merge into larger pieces in a process assisted by attached capping agent molecules, enclaving pores on the metal film. To investigate which formation mechanism dominates during nanopore formation, TEM images of nanopores were carefully examined, where we found that the latter mechanism is favored.

From the nanopore distribution in Figures 1 and 2, one finds that the characteristic structural features of nanopores, i.e., the diameter of 2−3 nm and separation at ∼20 nm, are much smaller than the light wavelength (800 nm). It is therefore unlikely that the disaggregation process would occur only at specific locations of the Ag film considering that all locations experience almost identical light field. Moreover, the smooth edge of the nanopores without any atom aggregation, seen in Figure 2b, also indicates that a disaggregation mechanism is unlikely, since other studies clearly show aggregation at pore edges when light-induced disaggregation takes place.[12,33]

On the other hand, the progressive growing mechanism is supported by the TEM image shown in Figure 2c. The nanostructure features marked by A, B, C, D, and E are a microchasm, a thin groove, an enclosing groove, a shrinking nanosized slit, and a circular nanopore, respectively. They can be understood as different formation stages for the observed nanopores. A connected sequence A → B → C → D → E naturally illustrates a possible pathway for the nanopore formation. A chasm at the edge of the growing film becomes narrower to form a groove, then the groove closes at the very edge of the film to form a narrow slit. The slit continues to shrink, progressing away from the film's edge. Finally the groove is closed almost completely, leaving only a circular pore on the film. The film is flat and smooth without a noticeable trace of growth at the place where the two sides of the groove merge. A nanopore (E) is thus formed. With such a mechanism, strong repulsive contact is essential in stopping the growing process and finally forming the pore. Due to the spatial symmetry, a perfectly round-shaped pore intrinsically gives maximum repulsive force, as compared with other-shaped pores. Thus perfectly round-shaped pores are more favorable in our mechanism and have been more frequently observed in our experiment.

The effects of capping agent molecules onto the morphology of silver nanostructures in LAL are examined, where the PVP molecules block nanoparticle aggregation and citrate molecules favor thin film growth (see Supporting Information). As a result, in the presence of both molecules, scattered small-area Ag thin film flakes are formed with abundant film edges available and nanopores can thus be formed from enclaves (with molecules inside) within the thin film during high-intensity laser ablation. Both PVP and citrate molecules are essential in this process: without them or with one of them alone does not produce any nanopores (see Supporting Information), further confirming the progressive growth mechanism of nanopore formation. We note that although PVP molecules unlikely directly participate in making nanopores or chemical reductions, their exact roles at the molecular scale in the progressive evolution of silver nanopores are still open and subject to future studies.

The pore depth, or the film thickness, has also been measured. We show an AFM image of the same sample in Figure 3, where the inset is the film thickness (∼3 nm) measured along the red line marked in the figure. Although the AFM tip cannot penetrate nanopores with a diameter as small as 2 nm, the slowly varying plateau extending 20−50 nm in the AFM line scan indicates that the film thickness is rather homogeneous. This is further confirmed by the TEM images in Figure 2, where no obvious image contrast is observed around the edges of the nanopores. Thus a clear aspect ratio (depth/diameter) of 1.5 is obtained for our method. This depth/diameter ratio is most desirable in various technology applications such as local probe image mask, and in biologically important measurements, e.g., single-molecule detection with high-quality pores made by ion beam lithography.[7]

To further reveal the underlying *microscopic* mechanism during the formation of these nanopores, in particular, the effects of capping agent molecules, we employ state-of-the-art first principles methods to investigate the interaction of silver surfaces with the capping agent molecules.

We first calculate how the capping citrate molecule binds onto the silver surface. For this we use the (111) surface of Ag as a model substrate, which is the most stable facet for silver films and

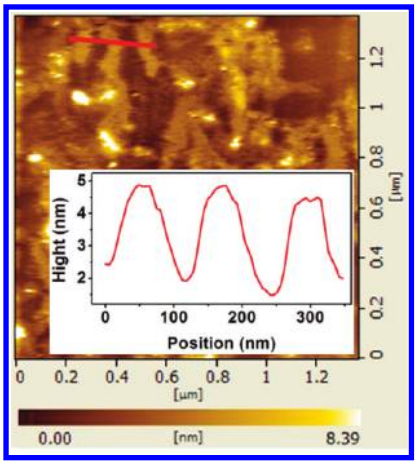

Figure 3. AFM image of Ag thin films produced using our LAL method. The inset shows the line scan of film thickness along the red bar shown in the AFM image. The maximum variation of ~3 nm in film thickness is observed. Note that nanopores are not visible in such a large scan area.

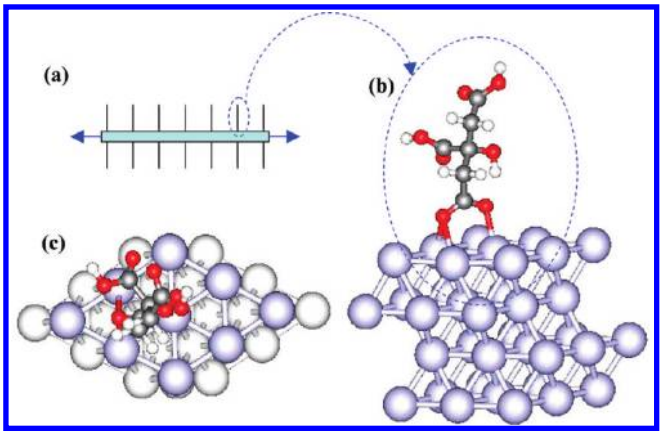

Figure 4. (a) Schematic illustration of a layer of capping agent molecules, citrate, on surfaces of silver thin film. Optimized geometry of a single citrate molecule adsorption on Ag(111) surface from first-principles calculations: side view (b), and top view (c). Big gray spheres represent silver atoms, smaller spheres with red, gray, and white colors represent oxygen, carbon, and hydrogen atoms, respectively.

evidenced during citrate-assisted thin film growth (Figure 4). Since we did not include the aqueous solution and counterions in our model, we use dihydrogen citrate[36] as a generally reasonable model for studying citrate adsorption. The most stable binding configuration in our calculations is the one where the dihydrogen citrate binds to surface Ag atoms via the end-carboxyl group forming three Ag−O bonds, namely, one oxygen atom was bound on the top site of Ag while the other oxygen sits on the bridge site. The Ag−O bond lengths are 2.35 Å (on top) and 2.49 and 2.54 Å (on bridge). The average vertical distance between oxygen atoms and the Ag surface is 2.43 Å along the surface normal. Moreover, the surface Ag atom right beneath the oxygen atom has been pushed into the slab by 0.1 Å because of the anticorrelation rule of surface adsorption.[37] This configuration is very stable, with a large adsorption energy calculated to be 2.7 eV. The strong binding indicates that the surface will be covered with a stable layer of citrate molecules at room or even higher temperatures. This layer is further stabilized if we take into the consideration that neighboring molecules standing up on the Ag surface will form multiple hydrogen bonds between each other via carboxyl groups.

Next, we consider the interaction between adsorbed molecular layers on two separate surfaces when they approach each other driven by relaxation (from laser pulse generated excited states) induced film growth. For this we use the dimer of citrate molecules in free space to model the interaction between surface adlayers. Figure 5 shows the atomic structure of citrate dimers interacting via different kinds of bonds and the interaction energy plotted as a functional of their separation. The separation is approximately measured by the surface-to-surface distance assuming that the noninteracting ends of the dimer are bound to two Ag (111) surfaces, respectively, with the molecule−surface distance as the one calculated above for a single molecule adsorption. From Figure 5 we found that if we assume two citrate molecules are interacting via two hydrogen bonds between the two carboxyl end-groups, the optimal surface-to-surface separation is ~20.2 Å with an interaction energy about 1.2 eV.

However, in aqueous solutions citrate molecules are likely deprotonated. The end carboxyl groups can either form a hydration shell or temporally bind with Na^+ cation from solution forming *dynamical* ionic bonds with other molecules. In this case, our calculations show that the optimal surface-to-surface distance for a Na-mediated citrate dimer (Figure 5A) is ~21.8 Å. This cation-mediated interaction is rather strong with a binding energy about 2.2 eV, suggesting such a stable structure can be formed. The resulted structure is highly dynamic due to the high hydration energy of Na^+ ions in solution but would be rather stable to sustain the ultrafast laser pulses and the nanopore formation processes, especially in a confined space. Forming such a structure does not exclude Na hydration with additional water molecules considering the coordination number of 5 for Na^+ in aqueous solutions,[38] but Na−citrate bonds are stronger than Na−water bonding (around 0.7 eV),[38] rendering an overall more stable structure than the simple Na−water hydration structure depending on concentration, pH, etc. Therefore it is possible for such structures existing in a short time and a local space. This structure is not charge balanced: Two citrate molecules with one Na^+ form a negatively charged complex (−1), and the charge neutrality can be maintained by forming hydration shells around these complexes and counterions (Na^+ or H_3O^+). To maintain charge balance of the complex, we also tried another structure with an additional H^+ binding to one of two COO groups. A stable, neutral, two-citrate complex can also be formed, although with a reduced dimension (surface-to-surface distance 20.9 Å) and strength (0.6 eV).

On the other hand, without the coordination of the sodium cations, the deprotonated carboxyl groups repel each other due to the strong Coulombic interaction between the two charged groups. This is confirmed by our calculation and the energy curve shown in Figure 5. The repulsion is quite long ranged, which gradually diminishes at a separation of about ~28 Å (9 Å between two carboxyl groups). The dimension of our model nanopore is 2.2 nm, in excellent agreement with that observed in experiment (2.2 ± 0.3 nm). In addition, taking into account thermodynamic fluctuations inside the potential wells and the possible diversity of formed citrate−dimer complexes presented in Figure 5, the distribution of nanopore diameters is quite narrow, ranging from 2.0 to 2.3 nm, again consistent with the observed narrow size distribution in Figure 1. The larger nanopores, whose diameter is ~3.1 nm, would be a result of stuffing

dx.doi.org/10.1021/nl201529d |*Nano Lett.* 2011, 11, 3251–3257

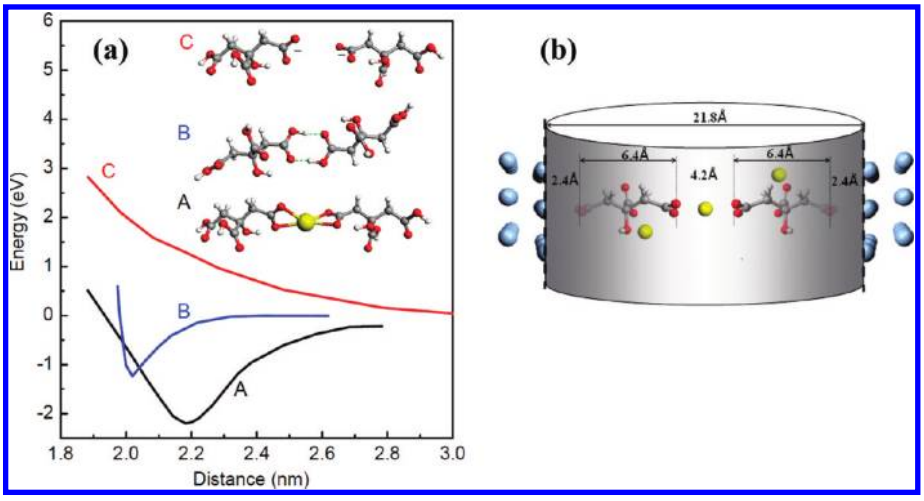

Figure 5. (a) Interaction between two citrate molecules via ionic bonds (A), hydrogen bonds (B), and Coulombic repulsive forces (C). Interaction energy as a function of molecular separation is plotted where the molecular separation is measured by the surface-to-surface distance between nanopore walls along the diameter direction. Inset: Optimized dimer structures corresponding to the above three cases. (b) Atomistic structural model for nanopores formed during laser ablation. Atomic distances from first-principles modeling are also depicted.

three connecting citrate molecules in a row into the pore region. We observe a much larger population of ~2 nm pores than ~3 nm pores in our experiment (Figure 1c), indicating dimer structures are more stable. This is because the molecule−surface interaction (2.7 eV) is much stronger than the average molecule−molecule interactions (≤2.2 eV).

Compared with light-illuminated chemical reduction experiments, we identify the essential role of intense femtosecond laser pulses in providing high enough transient excitations—high fluence in excitation results in more viable dynamical processes, and hence richer morphology in nanostructures. Here the preparation of silver atoms/ions and silver components is done within 80 fs and the formation of clusters, films, and nanopores is accomplished within longer time but much less than 10 min, whereas experiments of light-illuminated chemical reduction take hours. The instantly formed dense atoms/ions and silver components form a highly nonequilibrium excited state, which is absent in the regular chemical reduction methods. While the silver nanowires and nanotriangles observed in the chemical reduction methods have also been observed in our laser method,[39] we have observed this ultrasmall nanopore as an extra product, which is not accessible with current light-illuminated chemical reduction methods.

It is also instructive to compare our laser method with other currently available top-down technologies that can be used to make nanopores on metals. Well-defined nanopores of similar size (~2 nm) have been fabricated by Golovchenko, Dekker, and others, but on very different materials, such as insulating Si_3N_4 and SiO_2, and using very different methods, usually ion beam lithography and electron beam lithography.[7−10] To our knowledge we have not seen any metallic nanopores of such a small size being fabricated. To make a nanopore in metallic films, two of the most successful methods are ion-beam-induced deposition (with the smallest reported pore size for metal of slightly less than 10 nm[11]) and ultrafast laser near-field ablation (with the smallest reported pore size of 6 nm[12]); however, neither has been shown to be able to produce metal nanostructures as small as 2 nm. In Figure 6, we show TEM images of nanopores made with our modified LAL method, together with those made from TEM

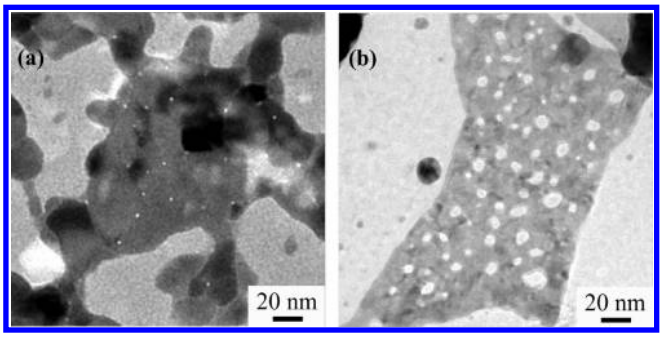

Figure 6. Comparison of nanopores fabricated by different methods: (a) the revised laser ablation in liquid method; (b) electron beam lithography using TEM.

beam lithography for comparison. The nanopores fabricated by electron beams are irregular in shape and randomly distributed, and the diameter distribution is much broader (ranging from 5 to 30 nm). Our revised LAL method has the advantages of making similar-sized nanopores with relatively larger distance between individual pores, and the silver film itself is undamaged. The high image contrast in Figure 6a between the nanopore region and the film, comparable to that in Figure 6b, implies that the molecules inside the pores might have been removed under electron beam illumination, leaving the nanopores empty. We emphasize that the 2 nm nanopore is the smallest in size among all those fabricated in metallic films with various methods including ultrafast laser near-field ablation, electron beam using TEM, and ion beam lithography. Needless to say, these methods have other advantages in fabricating single nanopores, such as being more determistic in spatial position and accessible to self-supporting membranes.

To further validate our experimental observation and confirm our proposed growth mechanism, we performed a parallel experiment using nearly identical experimental conditions except that the capping agent molecules are smaller molecules. If our proposed mechanism is correct, we should be able to see nanopores with a diameter controlled by the molecules' size.

dx.doi.org/10.1021/nl201529d |*Nano Lett.* 2011, 11, 3251–3257

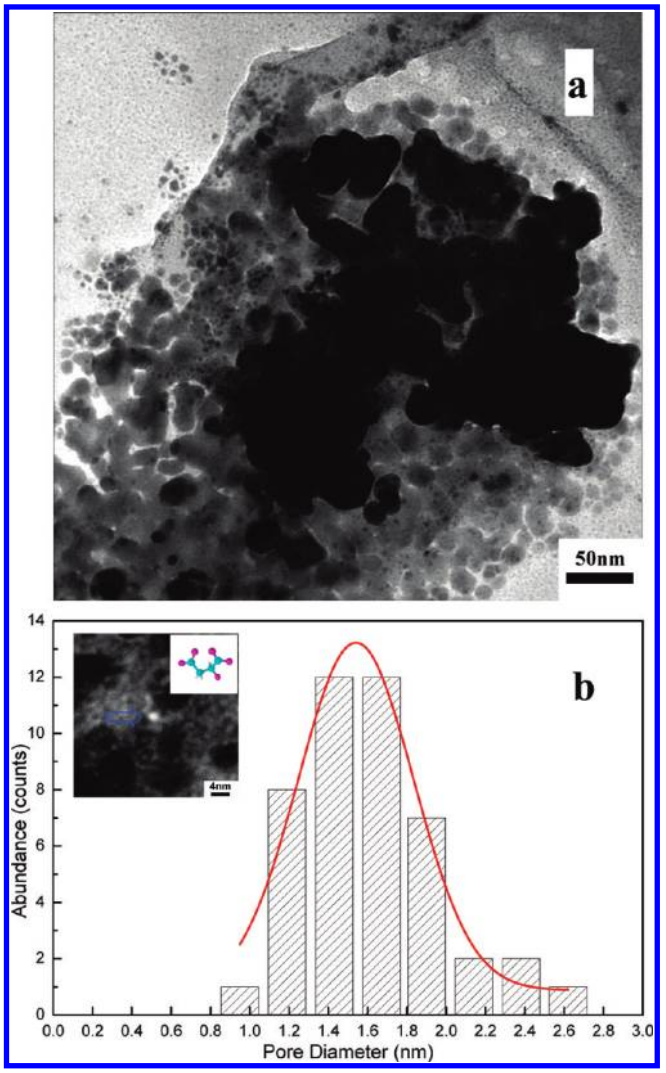

Figure 7. (a) TEM image of the thin film containing nanopores fabricated using LAL with assistance of PVP plus a different capping agent molecule, malate. (b) Histogram of the diameter distribution of the nanopores in (a). The red curve is a Gaussian fit of the diameter distribution as a guide to the eye. The inset of (b) shows a typical zoom-in view of such a nanopore. The upper left corner is a 3D ball-and-stick model of the malate ion. The blue arrow indicates the pore.

Here we chose a type of smaller molecule, sodium malate ($Na_2C_4H_4O_5$), which is a smaller molecule compared with sodium citrate. We added 0.3 mmol of malic acid ($C_4H_6O_5$, Alfa Aesar) and 0.6 mmol of sodium hydroxide (NaOH, Alfa Aesar) into 11.03 mL of deionized water (Milli-Q, Millipore Co.) to produce the solution of sodium malate. A drop of the solution was used on a piece of pH paper to make sure the solution is neutral. The actual laser power was 680 mW instead of 700 mW as before. The result is shown in Figure 7. The statistics show an average diameter of about 1.6 nm, which is smaller than that for the sodium citrate, 2.3 nm. This is due to smaller molecule size of sodium malate, based on our proposed growth mechanism. This experiment fully confirms our proposed growth mechanism. However further experiments on larger molecules are not successful so far after quite a few experiments. It might be that not enough experiments have been tried. This is understandable if we consider there are quite a few tuning parameters in the experiment, such as the concentration for PVP, the concentration for the larger molecule, the laser average power, and the molecule itself. Also possible is that, for larger and larger molecules, the growth mechanism is no longer valid. So far what we can conclude is that the growth mechanism is valid for molecules having a dimension close to that of citrate and malate.

It is expected that our method is not limited to silver and can be applied to other metals[24] and their alloys. Within our novel method, further investigation and optimization of the properties of the laser pulse trains, capping agents, and ablated materials are expected to result in more diverse morphologies (for example, see Supporting Information for a silver nanosized leaf obtained by carefully defocusing the laser beam). The ultrasmall nanopores we have made may have potential applications in a variety of areas, such as near-field aperture probes and imaging masks,[4] biosensing for single molecules,[6] possible growth of ultrathin-nanowires from seeds constrained inside nanopores, and photocatalysis. For biosensing and transport applications, usually empty nanopores in a large flake are needed. We note that the flake size of 50 nm in the present work would already be useful under certain circumstance, especially when they are transferred to and combined with other membranes and nanomaterials. Since silver flakes are easily mounted to other materials, we expect that such a combination is feasible. In addition, the citrate ions inside the pores can be removed by heating, light illumination, or dissolution using stronger solvents, since the energy for citrate−Ag interaction (2.7 eV) is much smaller than that for Ag−Ag interaction at surfaces (3.9 eV).

In conclusion, we have fabricated ultrasmall metallic nanopores using an optical method. The 2 nm diameter nanopores produced have smooth edges and are well-separated. The formation of this new morphology we realized relies on the combined advantages of ultrafast intense laser excitation and the confinement of capping agent molecules. The formation mechanism has been explored and a progressive growth mechanism is discovered, which is confirmed by our first-principles calculations. Our revised LAL method enriches possible morphologies of metal nanostructures that can be formed with optical methods and entails more potential technologically important applications.

■ ASSOCIATED CONTENT

Supporting Information. TEM images of nanostructures fabricated with and without citrate and/or PVP molecules and TEM image of a nanosized leaf produced in the same conditions except with carefully defocused laser beam during the laser ablation. This material is available free of charge via the Internet at http://pubs.acs.org.

■ AUTHOR INFORMATION

Corresponding Author

*E-mail: smeng@iphy.ac.cn; jmzhao@iphy.ac.cn.

Author Contributions

§These authors contributed equally.

■ ACKNOWLEDGMENT

We acknowledge useful discussion with X. H. Lu, N. Grady, Jennifer P Ogilvie, J. H. Zhou, J. J. Xu, X. Z. Zhang, and J. Q. Li. We acknowledge TEM assistance from X. A. Yang. This work was

financially supported by the Natural Science Foundation of China (Nos. 10704085, 10974246 for J.Z., No. 11074287 for S.M., and Nos.10625418, 10874233 for H.X.), MOST (Nos. 2007CB936800, 2009CB930700 for H.X.), and CAS (KJCX2-EW-W04 for H.X. and the hundred-talent program for S.M.).

REFERENCES

(1) Park, T.; Mirin, N.; Lassiter, J. B.; Nehl, C. L.; Halas, N. J.; Nordlander, P. *ACS Nano* **2008**, *2*, 25–32.
(2) Prikulis, J.; Hanarp, P.; Olofsson, L.; Sutherland, D.; Käll, M. *Nano Lett.* **2004**, *4*, 1003–1007.
(3) Rindzevicius, T.; Alaverdyan, Y.; Dahlin, A.; Hőők, F.; Sutherland, D. S.; Käll, M. *Nano Lett.* **2005**, *5*, 2335–2339.
(4) Veerman, J. A.; Otter, A. M.; Kuipers, L.; van Hulst, N. F. *Appl. Phys. Lett.* **1998**, *72*, 3115–3117.
(5) Howorka, S.; Cheley, S.; Bayley, H. *Nat. Biotechnol.* **2001**, *19*, 636–639.
(6) Gershow, M.; Golovchenko, J. A. *Nat. Nanotechnol.* **2007**, *2*, 775–779.
(7) Li, J.; Stein, D.; McMullan, C.; Branton, D.; Aziz, M. J.; Golovchenko, J. A. *Nature* **2001**, *412*, 166–169.
(8) Storm, A. J.; Chen, J. H.; Ling, X. S.; Zandbergen, H. W.; Dekker, C. *Nat. Mater.* **2003**, *2*, 537–540.
(9) Garaj, S.; Hubbard, W.; Reina, A.; Kong, J.; Branton, D.; Golovchenko, J. A. *Nature* **2010**, *467*, 190–193.
(10) Merchant, C. A.; Healy, K.; Wanunu, M.; Ray, V.; Peterman, N.; Bartel, J.; Fischbein, M. D.; Venta, K.; Luo, Z.; Johnson, A. T. C.; Drndić, M. *Nano Lett.* **2010**, *10*, 2915–2921.
(11) Chen, P.; Wu, M. Y.; Salemink, H. W. M.; Alkemade, P. F. A. *Nanotechnology* **2009**, *20*, 015302.
(12) Jersch, J.; Demming, F.; Dickmann, K. *Appl. Phys. A: Mater. Sci. Process.* **1997**, *64*, 29–32.
(13) Gattass, R. R.; Mazur, E. *Nat. Photonics* **2008**, *2*, 219–225.
(14) Plech, A.; Leiderer, P.; Boneberg, J. *Laser Photonics Rev.* **2009**, *3*, 435–451.
(15) Morales, A. M.; Lieber, C. M. *Science* **1998**, *279*, 208–211.
(16) Jin, R.; Cao, Y.; Mirkin, C. A.; Kelly, K. L.; Schatz, G. C.; Zheng, J. G. *Science* **2001**, *294*, 1901–1903.
(17) Jin, R.; Cao, Y. C.; Hao, E.; Métraux, G. S.; Schatz, G. C.; Mirkin, C. A. *Nature* **2003**, *425*, 487–490.
(18) Barcikowski, S.; Devesa, F.; Moldenhauer, K. *J. Nanopart. Res.* **2009**, *11*, 1883–1893.
(19) Menéndez-Manjón, A.; Jakobi, J.; Schwabe, K.; Krauss, J. K.; Barcikowski, S. *J. Laser Micro/Nanoeng.* **2009**, *4*, 95–99.
(20) Mafuné, F.; Kohno, J.; Takeda, Y.; Kondow, T.; Sawabe, H. *J. Phys. Chem. B* **2000**, *104*, 9111–9117.
(21) Tsuji, T.; Iryo, K.; Ohta, H.; Nishimura, Y. *Jpn. J. Appl. Phys.* **2000**, *39*, L981–L983.
(22) Barcikowski, S.; Menéndez-Manjón, A.; Chichkov, B.; Brikas, M.; Račiukaitis, G. *Appl. Phys. Lett.* **2007**, *91*, 083113.
(23) Kabashin, A. V.; Meunier, M.; Kingston, C.; Luong, J. H. T. *J. Phys. Chem. B* **2003**, *107*, 4527–4531.
(24) Barcikowski, S.; Hahn, A.; Kabashin, A. V.; Chichkov, B. N. *Appl. Phys. A: Mater. Sci. Process.* **2007**, *87*, 47–55.
(25) Xia, Y.; Halas, N. J. *MRS Bull.* **2005**, *30*, 338–348and references therein.
(26) Wiley, B.; Sun, Y.; Mayers, B.; Xia, Y. *Chem.—Eur. J.* **2005**, *11*, 454–463.
(27) Sun, Y.; Mayers, B.; Xia, Y. *Nano Lett.* **2003**, *3*, 675–679.
(28) Sun, Y.; Xia, Y. *Adv. Mater.* **2003**, *15*, 695–699.
(29) Chen, J.; Wiley, B.; Li, Z. Y.; Campbell, D.; Saeki, F.; Cang, H.; Au, L.; Lee, J.; Li, X.; Xia, Y. *Adv. Mater.* **2005**, *17*, 2255–2261.
(30) Soler, J. M.; Artacho, E.; Gale, J. D.; García, A.; Junquera, J.; Ordejón, P.; Sánchez-Portal, D. *J. Phys.: Condens. Matter* **2002**, *14*, 2745–2779.
(31) Troullier, N.; Martins, J. L. *Phys. Rev. B* **1991**, *43*, 1993–2006.
(32) Perdew, J. P.; Burke, K.; Ernzerhof, M. *Phys. Rev. Lett.* **1996**, *77*, 3865–3868.
(33) Preuss, S.; Demchuk, A.; Stuke, M. *Appl. Phys. A: Mater. Sci. Process.* **1995**, *61*, 33–37.
(34) Perez, D.; Lewis, L. J. *Phys. Rev. Lett.* **2002**, *89*, 255504.
(35) Kabashin, A. V.; Meunier, M. *J. Phys.: Conf. Ser.* **2007**, *59*, 354–359.
(36) Shafeeuulla Khan, M. A.; Sen, A.; Ganguly, B. *CrystEngComm.* **2009**, *11*, 2660–2667.
(37) Meng, S.; Xu, L. F.; Wang, E. G.; Gao, S. W. *Phys. Rev. Lett.* **2002**, *89*, 176104.
(38) Meng, S.; Chakarov, D. V.; Kasemo, B.; Gao, S. W. *J. Chem. Phys.* **2004**, *121*, 12572–12576.
(39) Bian, F.; Wang, R.; Yang, H. X.; Zhang, X. Z.; Li, J. Q.; Xu, H. X.; Xu, J. J.; Zhao, J. M. *Chin. Phys. Lett.* **2010**, *27*, 088101.